International Forum on Aeroelasticity and Structural Dynamics
IFASD 2024
17-21 June 2024, The Hague, The Netherlands

NONLINEAR AEROELASTIC ANALYSIS OF A REGIONAL AIRLINER WING VIA A NEURAL-NETWORK BASED REDUCED ORDER MODEL FOR AERODYNAMICS

Nicolò Laureti[1], **Luca Pustina**[1], **Marco Pizzoli**[1], **Francesco Saltari**[1], **Franco Mastroddi**[1]

[1]Dept. of Mechanical and Aerospace Engineering
Sapienza University of Rome
Via Eudossiana 18, 00184 Rome, Italy

Keywords: nonlinear aeroelasticity, neural network, reduced-order models

Abstract: This paper investigates the use of a neural network based reduced order model to solve the nonlinear gust response of a regional aircraft wing characterised by high angle of attack and gust intensity. Dynamic aerodynamic stall is generally able to provide a natural load mitigation, which is generally not considered in aircraft design. The neural network is combined with strip theory, thus requiring the training of a single airfoil model. Given the difficulties in obtaining CFD based aerodynamic data due to the excessive time consuming simulations, the approach has started the training phase with data obtained from the Beddoes-Leishman unsteady aerodynamic model. The wing response is then evaluated by a reduced-order model implemented in the Simulink environment, based on Nastran structural data and strip theory, enhanced by a number of neural networks in parallel describing the nonlinear transient behavior.

NOMENCLATURE

S	loads integration matrix
α_0	trim angle of attack
$\bar{q}^{(j)}$	non-dimensional *j*-th strip pitch rate
$\bar{w}^{(j)}_{3/4}$	non dimensional velocity at 3/4 chord
χ	modified normalwash vector
$\mathbf{u}$	displacement field
$\mathbf{x}$	position vector
ω	angular frequency
ω_n	*n*-th modal angular frequency
$\boldsymbol{\psi}_n$	*n*-th mode shape
$\mathsf{A}_0, \mathsf{A}_1$	non-circulatory contributions of the inverse of influence matrix
$\mathsf{B}_0, \mathsf{C}, \mathsf{P}, \mathsf{B}$	matrices providing the circulatory contribution of the inverse of influence matrix
c	aerodynamic coefficient vector

C_α matrix enabling the description of 3D finite wing effect

$\mathsf{D}^{(1)}, \mathsf{D}^{(2)}$ real and imaginary parts of differentiation matrix

d_g static angle of attack and gust input vector

e generalized force vector

K modal stiffness matrix

M modal mass matrix

q generalized coordinate vector

r aerodynamic state vector

σ standard deviation of the power spectral density

τ reduced time

A_h, A_α variance of the power spectral densities of pitch and plunge

b semi-chord

$c_n^{(j)}$ lift coefficient of the *j*-th strip

$c_m^{(j)}$ moment coefficient of the *j*-th strip

k reduced frequency

L_g gust lenght

M_∞ Mach number

N number of modes

P number of strips

q_D dynamic pressure

$q_n(t)$ *n*-th generalized coordinate

S_α, S_h power spectral density for pitch and plunge

t time

U_∞ free stream velocity

w_{g_a} gust velocity amplitude

1 INTRODUCTION

Climate change and the increasing scarcity of resources necessitate a significant reduction in aviation impact on both citizens and the environment. Reducing greenhouse gas emissions is one of the most important challenges currently facing the aviation industry, where even a relatively modest reduction in aircraft weight can result in a significant reduction in fuel consumption. Thus, the reduction of weight is critic not only to lower CO2 emissions but also to decrease the costs associated with the aircraft operations [1]. Aircraft manufacturers are striving to develop aircraft that are more efficient and at the same time have a reduced structural weight, with the aim of reducing their environmental impact on the one hand and their manufacturing and operating costs on the other.

However, the use of standard methods for determining structural loads based on linear aeroelastic models can result in the over-sizing of structural elements in order to ensure a sufficient safety margin. Specifically, There are several physics within the aeroelastic dynamics of the wing that are likely to reduce wing loads during very intense (design) gusts, which are neglected due to modeling complexity and treated by extremely conservative approaches. These include sloshing within the wing tanks, which has the ability to increase the structural damping of the wing, and dynamic stall, which can occur in flight conditions characterized by high angle of attack and intense gust inputs. Among the most commonly employed aerodynamic models is the doublet lattice method [2]. This method has been used to construct a three-dimensional aerodynamic model, offering enhanced accuracy in the evaluation of lift for low angles of attack. Consequently, this approach is suitable for aeroelastic analysis and accounting for finite wake effects. However, as a potential aerodynamic model, the model lacks the capacity to represent both static and dynamic stall effects. This limitation restricts the model ability to assess loads in the points of the flight envelope that are close to the stall curve.

To explore more complex aerodynamic scenarios, CFD methods based on the Navier-Stokes equations can be utilized, as they offer high precision in analysis. Previously computationally intensive, advancements in computational capabilities have significantly reduced the required effort, making these analyses increasingly common in aircraft design [3]. However, their application in a coupled fluid-structure interaction (FSI) loop at high angles of attack remains computationally prohibitive during the preliminary design phase. The complexity of dynamic stall further complicates its prediction, often necessitating specific wind tunnel experiments to assess its effects accurately. Moreover, for modern flexible aircraft withstanding atmospheric perturbation like vertical gust means both elastic and rigid body modes are exited, inducing unexpected additive structural loads and reduce structural fatigue life. To the end of alleviate gust loads and reduce wing root bending moment, there is increasing interest in designing nonlinear controllers, [4], [5] based on aerodynamic models accounting for nonlinearities that activate at high angle of attack [6].

The objective of this study is to demonstrate the viability of training neural network reduced-order models for estimating aerodynamic forces at high angles of attack, considering both static and dynamic stall effects. This approach potentially enables a more accurate evaluation of aerodynamic loads at the points of the flight envelope featured by high angle of attack, facilitating the design of lighter structures. The numerical testbed consists of a typical 42-seat regional aircraft. The present approach aims at comparing the load-relieving effects of dynamic stall with the prediction provided by the linear aeroelastic model based on the strip theory. Due to the time constraints associated with CFD data, aerodynamic data derived from the more practical Beddoes-Leishman model were employed. However, the medium term goal is to apply the

developed methodology training the surrogate aerodynamic model based on neural networks using CFD-derived data.

In recent years, reduced-order models leveraging neural networks have been employed to predict nonlinear, unsteady aerodynamics with notable accuracy and computational efficiency. This need has emerged from the necessity to balance precision and computational resource consumption, addressing the inefficiencies inherent in CFD-based techniques. The advent of architectures such as long-short term memory (LSTM) networks has enabled the effective modeling of time-delay phenomena characteristic of aeroelasticity, making this domain a prime candidate for such approaches. Various neural network models have been developed with this objective, although the need to accurately characterize both linear and nonlinear dynamics results in varying performance across different architectures. For instance, recurrent neural networks (RNNs) have been applied to predict limit-cycle oscillations (LCO) at specific Mach numbers [7]. Additionally, LSTM networks have demonstrated good performance in applications involving 2D airfoils in the transonic regime at varying Mach numbers, successfully adapting to different problem parameters [8]. On the other hand, the authors employed a methodology exploiting neural network for sloshing to obtain the aeroelastic response of a wing prototype to gusts when stowing sloshing fuel [9]. The neural network was trained by experimental data to return vertical force at the tank location based on the vertical velocity of the tank. When accounting for several compartments along the wing span this results in a sort of strip theory for sloshing with neural network model. This approach enabled the optimization of fuel consumption strategy to minimize gust-induced internal loads [10].

As mentioned before, in this inital phase of the methodology development, the aerodynamic data were obtained using Beddoes-Leishman model [11], originally developed for helicopter blade applications. It is a semi-empirical approach specifically designed to address a particular aerodynamic phenomena such as dynamic stall featuring the separation of the flow at the leading and trailing edges and the dynamic vortex. Over the years, a manifold of variants of the Beddoes-Leishman model have been introduced for different applications, typically involving parameter tuning to fit with experimental data [12]. These models are used across various engineering fields where dynamic stall is a critical design factor, such as in helicopter rotor blades and wind turbine blades [13]. In this work, a recursive model of Beddoes-Leishman [14] is employed were the description of the attached flow is described via an indicial formulation [15]. In order to assess the dynamic loads exerted on a wing subjected to intense gusts, an approach combining neural networks and strip theory was employed. More specifically, the approach starts from the generation of a proper dataset using unsteady response of a 2D airfoil to random input with spectral characteristics specifically addressing the gust load response. The dataset, obtained using Beddoes-Leishman nonlinear aerodynamic model is subsequently used to train a long short term memory model. Both Beddoes-Leishman model and the neural-network based ROM are then integrated within a strip theory approach in order to provide the response of aircraft to intense gust loads and quantify the natural alleviation of loads that this model is able to retrieve.

The paper is organized as it follows. The aeroelastic formulation is introduced in Sec. 2 whereas the collection of data via Beddoes-Leishman model as well as the training are provided in Secs. 3 and 4, respectively. The results are illustrated in Sec. 5 and finally a concluding remarks section ends the paper.

2 AEROELASTIC FORMULATION

The aeroelastic wing is modeled in this work using a hybrid model that combines a linear differential problem with a data-driven model for dynamic stall. More in details, the numerical testbed is represented by a regional aircraft wing model represented in Fig. 1 through its finite element model and aerodynamic strips.

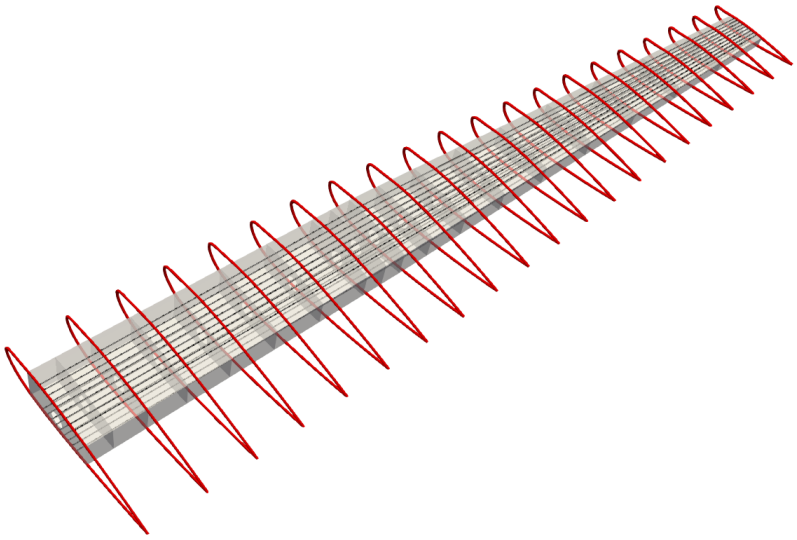

Figure 1: Regional aircraft wing model.

On the other hand, Fig. 2 shows the first six modes of vibration of the wing structure. Therefore, the wing structural displacements $\mathbf{u}(\mathbf{x}, t)$ can be expressed by the following spectral decomposition:

$$\mathbf{u}(\mathbf{x}, t) \simeq \sum_{n=1}^{N} \boldsymbol{\psi}_n(\mathbf{x}) q_n(t) \tag{1}$$

where $\boldsymbol{\psi}_n(\mathbf{x})$ are the modes of vibrations of the structure and $q_n(t)$ are the generalized coordinates describing the body deformation in time. Note that a space-discretization for the structure is assumed by including a finite number N of modes in the analysis, *i.e.,* a frequency-band-limited unsteady process. Considering this representation for aircraft wing dynamics, one has the following Lagrange equations of motion in terms of N modal coordinates $q_n(t)$

$$\mathsf{M}\ddot{\mathsf{q}} + \mathsf{K}\mathsf{q} = \mathsf{e} \tag{2}$$

where $\mathsf{q} = [q_1, q_2, \ldots, q_N]^\mathsf{T}$ is the modal coordinates vector, M and K are, respectively, the modal mass and stiffness (diagonal) matrices provided by the finite element solver, whereas $\mathsf{e} = [e_1, e_2, \ldots, e_N]^\mathsf{T}$ is the vector of the generalized aerodynamic forces. The generalized aerodynamic forces are generally computed as a function of the reduced frequency $k = \omega b / U_\infty$ (with b semi-chord and U_∞ free stream velocity) and Mach M_∞ domain. This methodology exploits the strip theory that, defining as $\mathsf{c} = [c_n^{(1)}, c_m^{(1)}, c_n^{(2)}, c_m^{(2)}, \ldots, c_n^{(P)}, c_m^{(P)}]^\mathsf{T}$ the vector collecting the aerodynamic lift and moment coefficients at 1/4 of the chord for the P strips as a function of time, provides in Fourier domain:

$$\tilde{\mathsf{e}} = q_D \, \mathsf{S} \, \tilde{\mathsf{c}} \tag{3}$$

where S is a matrix that projects the strip loads onto the generalized modes. On the other hand, it is defined the modified normalwash vector $\chi = [\bar{w}_{3/4}^{(1)}, \bar{q}^{(1)}, \bar{w}_{3/4}^{(2)}, \bar{q}^{(2)}, \ldots, \bar{w}_{3/4}^{(P)}, \bar{q}^{(P)}]^\mathsf{T}$ used to

list the non-dimensional velocity at $3/4$ of the chord and the non-dimensional pitch rate of the P strips such that:

$$\tilde{\chi} = \mathsf{C}_\alpha \Big(\big(\mathsf{D}^{(1)} + ik\mathsf{D}^{(2)} \big) \tilde{\mathsf{q}} + \mathsf{d}_g (\alpha_0 + \frac{w_g}{U_\infty}) \Big) \tag{4}$$

where α_0 is trim angle of attack and w_g is the gust velocity and the matrix C_α allows to approximate the 3D finite-wing aerodynamics effect. Specifically, the latter is obtained via the Prandtl lifting line theory.

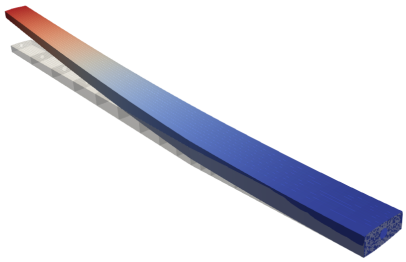

(a) 1^{st} O-P-B

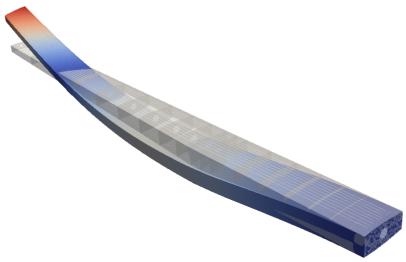

(b) 2^{nd} O-P-B , $\omega_2/\omega_1 = 3.35$

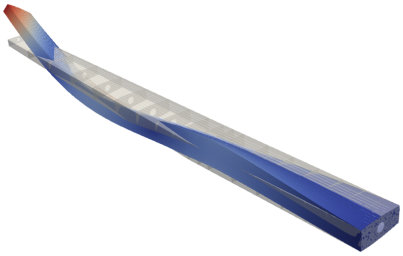

(c) 2^{nd} O-P-B / 1^{st} T, $\omega_3/\omega_1 = 6.06$

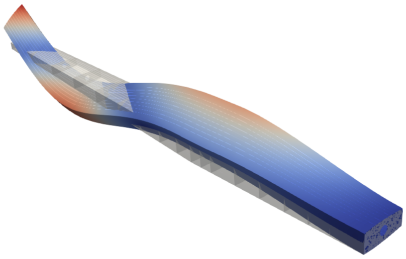

(d) 3^{rd} O-P-B / 1^{st} T, $\omega_4/\omega_1 = 9.94$

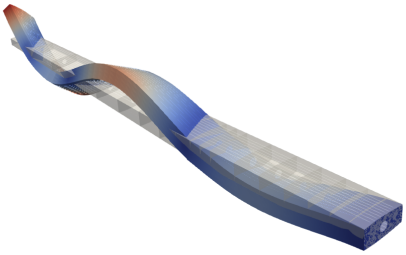

(e) 4^{rd} O-P-B / 1^{st} T, $\omega_5/\omega_1 = 16.26$

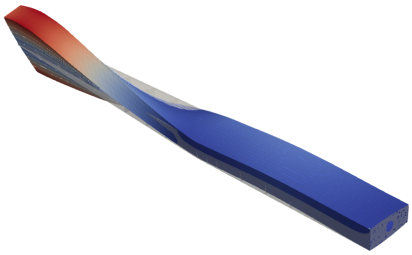

(f) 1^{st} T, $\omega_6/\omega_1 = 19.93$

Figure 2: Mode shapes of the wing model with their natural frequencies. O-P-B = Out-of-plane bending mode, I-P-B = In plane bending mode, T = torsional mode.

The relationship between the linear (attached flow) aerodynamic coefficients $\tilde{\mathsf{c}}^{(lin)}$ and the wing

velocity field χ can be expressed via the functions introduced in Refs. [15, 16] and hereafter recast in rational-polynomial matrix form:

$$\tilde{\mathsf{c}}^{(lin)} = \left(\mathsf{A}_0 + \mathsf{B}_0 + ik\mathsf{A}_1 + \mathsf{C}\big(ik\mathsf{I} + \mathsf{P}\big)^{-1}\mathsf{B}\right)\tilde{\chi} \tag{5}$$

where A_0 and A_1 are non-circulatory terms whereas B_0 and $\mathsf{C}\big(ik\mathsf{I}+\mathsf{P}\big)^{-1}\mathsf{B}$ allow to describe the circulatory aerodynamics. The previous equation can be recast in time domain by introducing the vector of aerodynamic states r as:

$$\mathsf{c}^{(lin)} = \left(\mathsf{A}_0 + \mathsf{B}_0\right)\chi + \frac{b}{U_\infty}\mathsf{A}_1\,\dot{\chi} + \mathsf{C}\,\mathsf{r} \tag{6}$$

$$\dot{\mathsf{r}} = \frac{U_\infty}{b}\mathsf{P}\,\mathsf{r} + \frac{U_\infty}{b}\mathsf{B}\,\chi \tag{7}$$

The linear aeroelastic modeling is implemented in Simulink® as illustrated in Fig. 3. The *structure* block translates Eq. 2, whereas the aerodynamic block is deepened in the bottom part of the figure detailing the circulatory and non-circulatory aerodynamics.

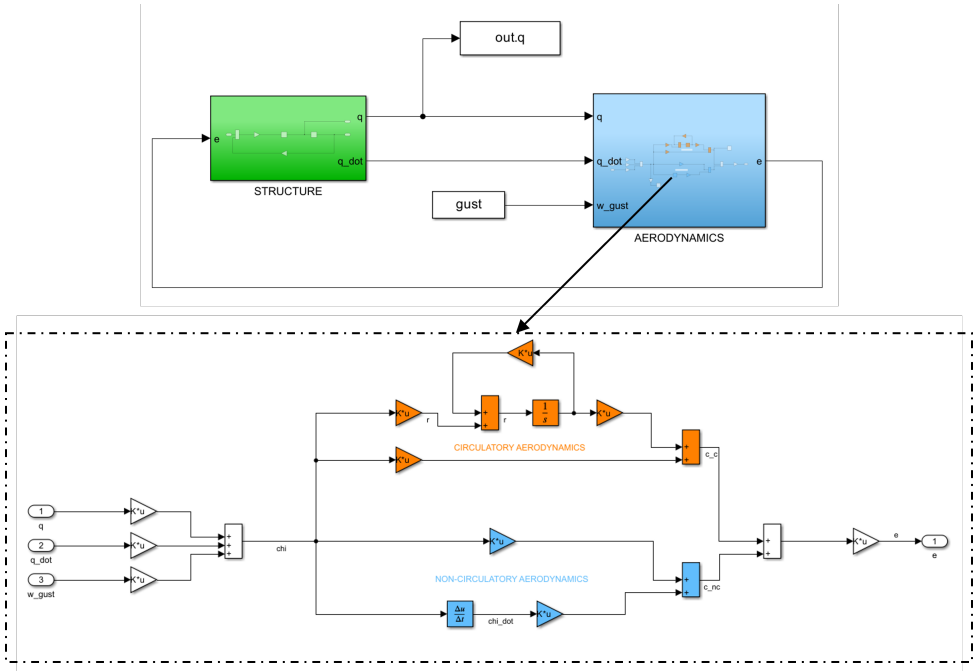

Figure 3: Linear aeroelastic modeling in Simulink®.

To represent the aerodynamic nonlinear effects resulting from dynamic stall, this approach makes use of the semi-empirical Beddoes-Leishman model. This model facilitates the representation of vortex onset at the leading edge due to dynamic stall and enables empirical evaluation of its impact on aerodynamic coefficients. Furthermore, nonlinear effects resulting from vortex detachment at the trailing edge can be incorporated using Kirchhoff's theory. This theory introduces a correction to the aerodynamic coefficients associated with the flow detachment point from the trailing edge, a condition contingent on the behavior of the profile. For these reasons, the Beddoes-Leishman model can be employed as a replacement of CFD simulations for obtaining datasets to be used for the neural-network training. While this approach results in lower accuracy, it offers a significant reduction in computational cost at this stage of methodological development. So it is possible to obtain data to train the neural-network model and for

the implementation of a reference nonlinear aeroelastic model to assess the performance of the hybrid modeling including neural-network. Neglecting for the sake of conciseness the details about the formulation, the BL model allows to update $c_n^{(j)}$ and $c_m^{(j)}$ in cascade with respect to the evaluation of the linear (attached flow) $c_n^{(lin)_j}$ and $c_m^{(lin)_j}$ and local angle of attack α_j such that for the *j*-th profile, one has:

$$\begin{Bmatrix} c_n^{(j)} \\ c_m^{(j)} \end{Bmatrix} = f\left(c_n^{(lin)_j}, c_m^{(lin)_j}, \alpha_j \right) \tag{8}$$

This can be noticed from the green block in Fig. 4, that is detailed in the bottom part of the figure. Note that a programmatic Simulink compiler allows the nonlinear aerodynamic response to be replicated for as many dynamics as the number of strips.

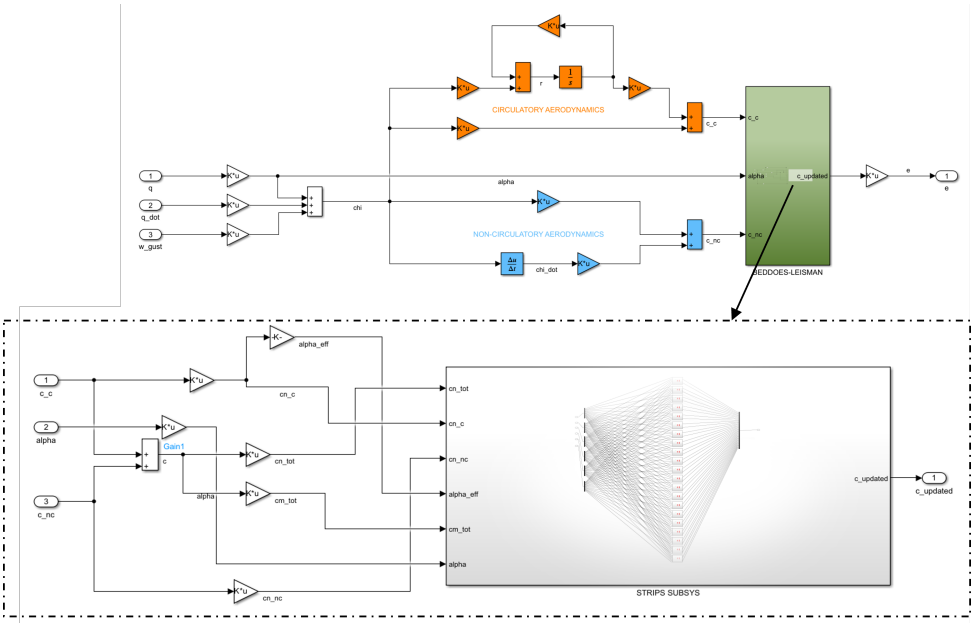

Figure 4: Beddoes-Leishman-based non-linear aerodynamic implementation in Simulink®.

On the other hand, the nonlinear aerodynamic contribution can be provided by neural-network reduced order model that provides a correction of the lift and moment coefficient vectors $\Delta c_n^{(j)}$ and $\Delta c_m^{(j)}$ as a function of the velocities on each profile $\bar{w}_{3/4}^{(j)}$ and $\bar{q}^{(j)}$.

$$\begin{Bmatrix} c_n^{(j)} \\ c_m^{(j)} \end{Bmatrix} = \begin{Bmatrix} c_n^{(lin)_j} \\ c_m^{(lin)_j} \end{Bmatrix} + \begin{Bmatrix} \Delta c_n^{(j)} \\ \Delta c_m^{(j)} \end{Bmatrix} \tag{9}$$

This operation is performed in parallel with the evaluation of the linear aerodynamic coefficient vector c, as provided by Fig. 5. Again, a programmatic Simulink compiler enables to replicate the neural network for each strip. Moreover, since the model is trained in reduced time domain, rate transition blocks enable to adapt the time step of each strip in order to account for the local chord length (see Fig. 6). The description of such approach based on neural network to describe Δc_n and Δc_m is covered in Sec. 4.

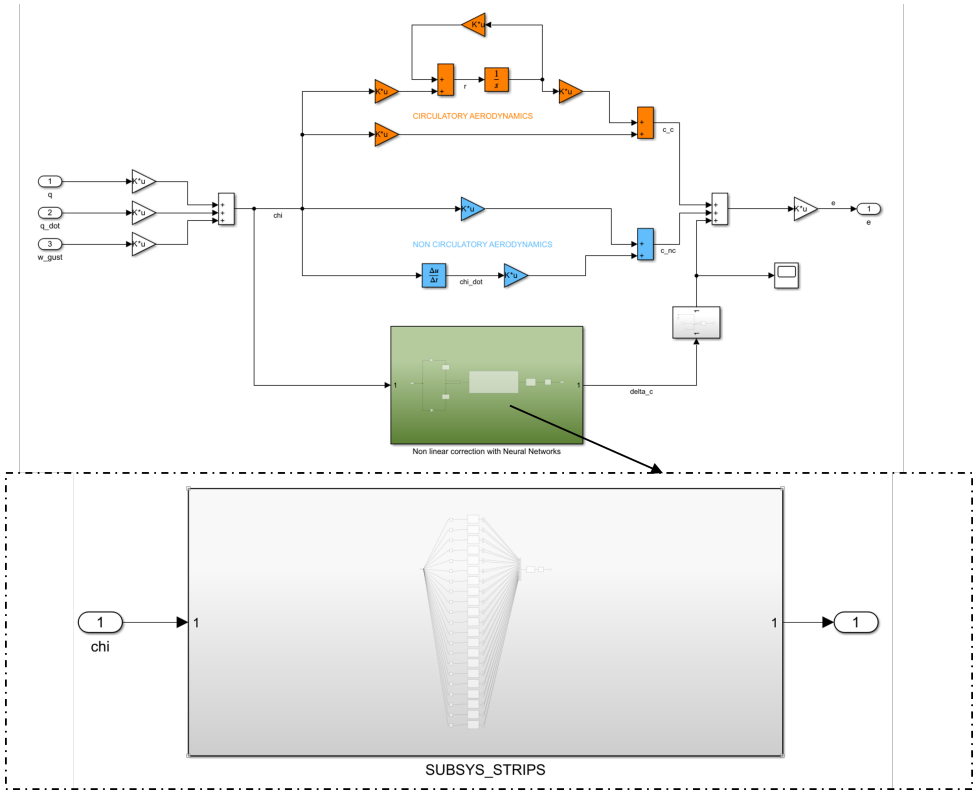

Figure 5: Neural-network based non-linear aerodynamic implementation in Simulink®.

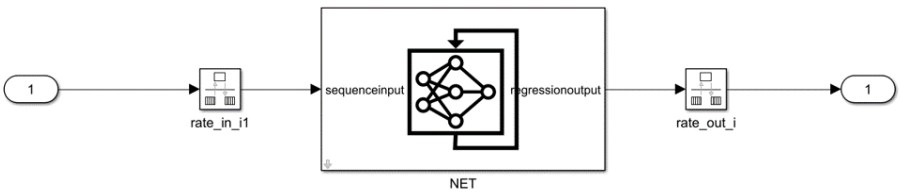

Figure 6: Rate transition blocks enabling the dilation of time in Simulink®.

3 DATA COLLECTION FROM BEDDOES-LEISHMAN MODELING

This section provides a description of the dataset used for training a neural network-based model for describing nonlinear airfoil behavior due to dynamic stall. The dataset was obtained by means of the Beddoes-Leishman aerodynamic model, although a CFD model can be used if sufficient computing resources are available.

The training dataset must consist of randomly generated data that reflects the specific application case being studied. In this study, the application involves simulating intensive vertical gusts encountered during the landing approach or initial phase of climb for a generic regional airplane. In this work, the training process involved creating a dataset composed of forty random inputs for the single-airfoil model, with twenty inputs allocated for the training phase and twenty for the validation. The input data are organized in terms of normalwash $\chi^{(j)}$ as a function of the reduced time $\tau = tU_\infty/b$ where the superscript $^{(j)}$ is avoid when expressing training dataset. The random signals representing $\bar{w}_{3/4}$ and $\bar{q}$ are generated using the more familiar variables of

pitch α and plunge h/b used through the following relation:

$$\begin{Bmatrix} \bar{w}_{3/4}(\tau) \\ \bar{q}(\tau) \end{Bmatrix} = \begin{Bmatrix} \alpha_0 \\ 0 \end{Bmatrix} + \begin{Bmatrix} \alpha(\tau) + \frac{\mathrm{d}}{\mathrm{d}\tau}\frac{h}{b} \\ 2\frac{\mathrm{d}}{\mathrm{d}\tau}\alpha \end{Bmatrix} \tag{10}$$

where $\alpha(\tau)$ and $h(\tau)/b$ are obtained as a realization of their respective Power Spectral Density (PSD) Gaussian-like function $S_h(k)$ and $S_\alpha(k)$:

$$S_\alpha(k) = 2\frac{A_\alpha}{\sigma\sqrt{2\pi}}\, e^{-\frac{k^2}{\sigma^2}} \qquad\qquad S_h(k) = 2\frac{A_h}{\sigma\sqrt{2\pi}}\, e^{-\frac{k^2}{\sigma^2}} \tag{11}$$

that encompasses a frequency band that includes the first bending modal frequency of the wing, through its standard deviation imposed equal to $\sigma = 0.1885$.

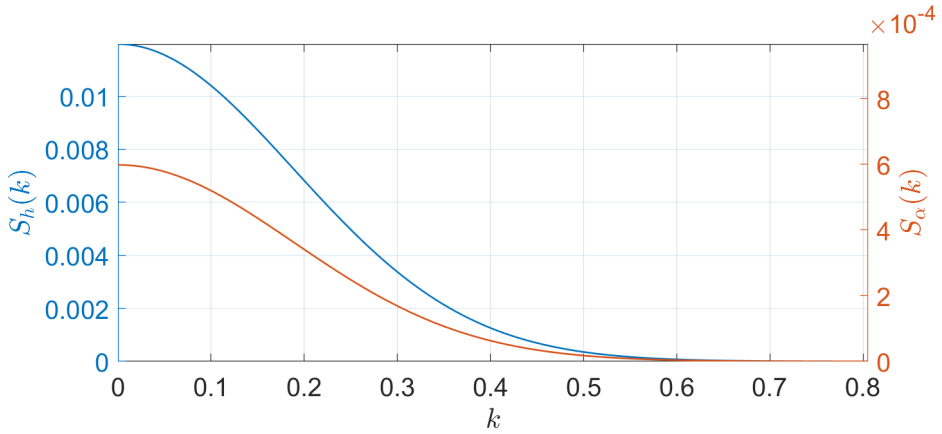

Figure 7: Power Spectral Density of pitch and plunge in the case of $A_h = 4.5 \cdot 10^{-2}$ and $A_\alpha = 2.3 \cdot 10^{-2}$.

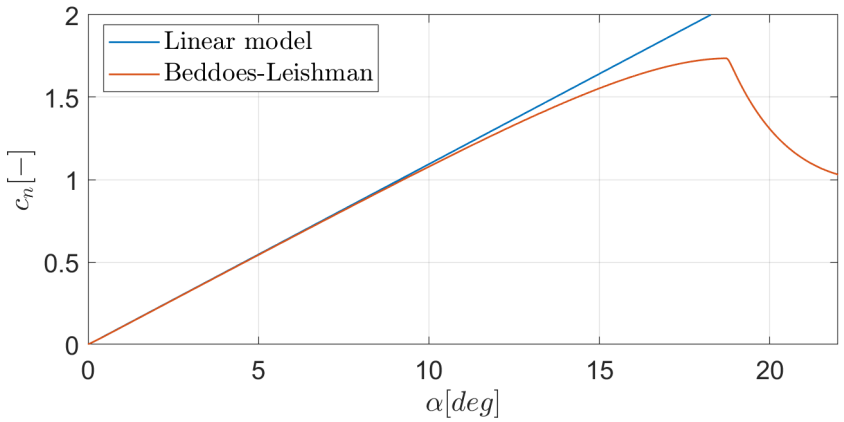

Figure 8: Stall curve of the airfoil NACA 0012.

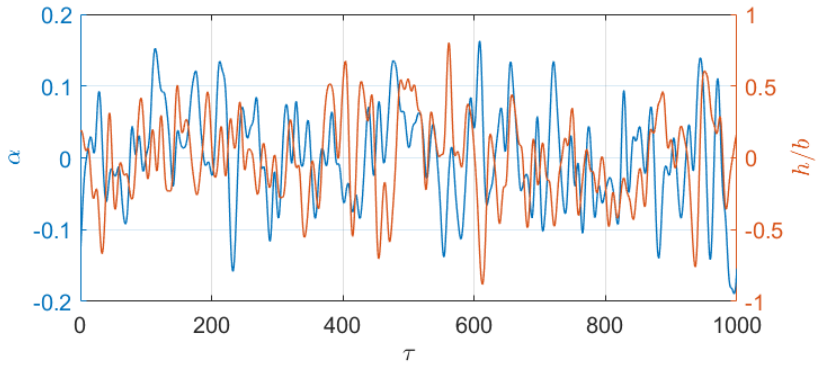

(a) $\alpha(\tau)$, $h(\tau)/b$

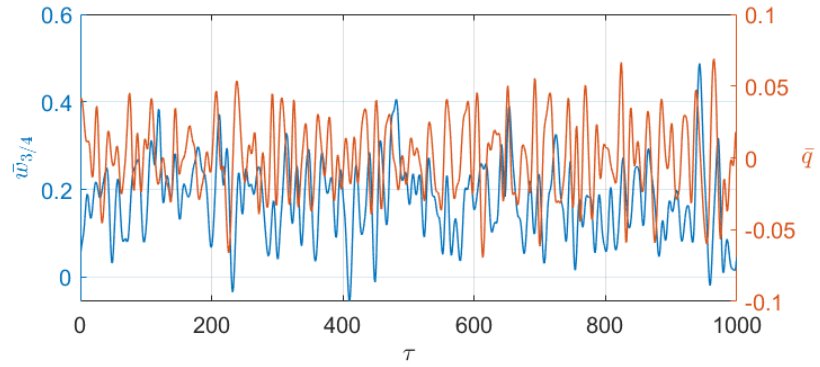

(b) $\bar{w}_{3/4}(\tau)$, $\bar{q}(\tau)$

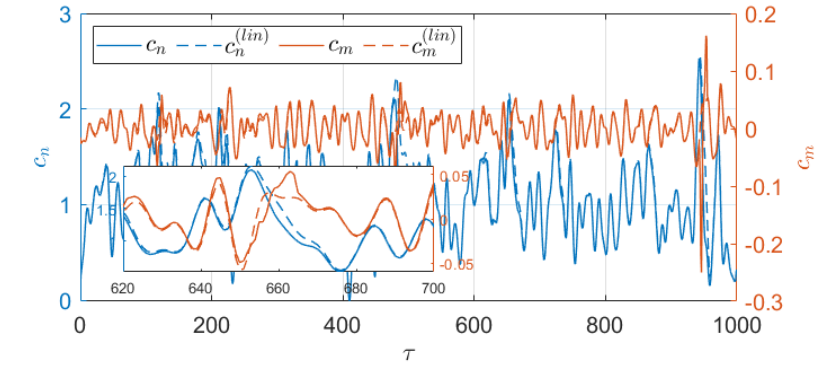

(c) c_n, $c_n^{(linear)}$, c_m, $c_m^{(linear)}$

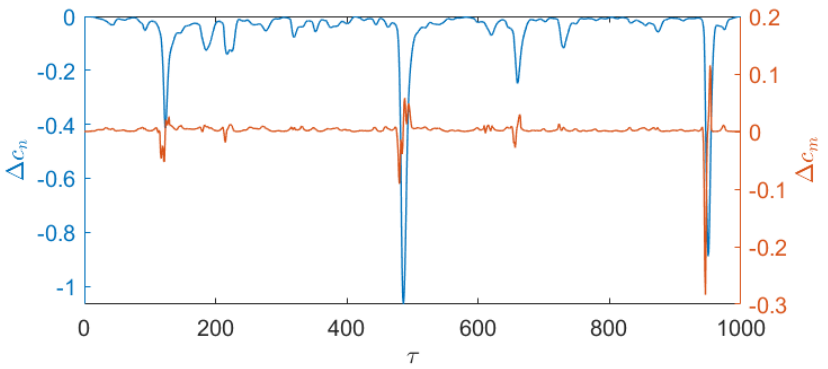

(d) Δc_n, Δc_m

Figure 9: Example of dataset generation for $\alpha_0 = 10\,deg$, $A_h = 4.5 \cdot 10^{-2}$ and $A_\alpha = 2.3 \cdot 10^{-3}$.

$\alpha_0[deg]$	A_α	A_h
0	$1.0 \cdot 10^{-5}$	$2.0 \cdot 10^{-4}$
5	$6.25 \cdot 10^{-5}$	$1.3 \cdot 10^{-3}$
10	$2.5 \cdot 10^{-4}$	$5.0 \cdot 10^{-3}$
15	$1.0 \cdot 10^{-3}$	$2.0 \cdot 10^{-2}$
	$2.3 \cdot 10^{-3}$	$4.5 \cdot 10^{-2}$

Table 1: Values of α_0 and amplitudes of PSD used for creating dataset for training.

In this specific study, our primary interest lies in the plunge motion influenced by the wing response to gusts. The amplitude of the PSD signal for the plunge motion and the initial airfoil trim angle (denoted as α_0) were used for the realization of the time histories. To construct the dataset, five different amplitudes of the PSD were employed for the plunge signal and four distinct values of the trim angle α_0, as it is possible to see in table [1]. For each initial angle of attack, five timeseries of the plunge and pitch are made, respectively, one for each amplitude of the PSD. The amplitude relationship between the PSD for plunge and pitch is governed by a scale factor, indicating that the plunge signal PSD amplitude is ten times greater than that of the pitch signal, as it can be noticed in Fig. 7 and from the second and third column of table [1].

The realization of the signals for α and h ensures their mutual uncorrelation. On the other hand, the values of α_0 are evaluated on the basis of a stall curve of the airfoil considering the nonlinear effect provided by Beddoes-Leishman model, as it can be noticed from Fig. 8. The chosen values explore different flow regimes around the profile. Lower values, even under gust conditions, allow the generation of datasets for the network that adequately explore the linear behavior of the aerodynamics, while higher angle of attack values, thus closer to a stall condition, allow, depending on the intensity of the gust, the generation of a dataset that contains information on the nonlinear corrections obtained using the Beddoes-Leishman model. Figure 9 resumes the workflow for the generation of the dataset. The time series of α and h/b are generated from their respective variance in Fig. 9(a). These signals, along with the steady angle of attack α_0 provides the normalwash in terms of $\bar{w}_{3/4}$ and $\bar{q}$ in Fig. 9(b), that is, the input dataset for the neural network model training. Afterwards, the simulations provide the resulting c_n and c_m in Fig. 9(c) that finally allows the computation of Δc_n and Δc_m in Fig. 9(d) that consists of the output dataset for the training.

4 NEURAL-NETWORK TRAINING

Scope of the neural-network based reduced order model is to provide the nonlinear contribution to the lift and moment coefficients of each strip. These two outputs of the model are obtained by considering the reduced time τ history of the non-dimensional down-wash at 3/4 chord and the pitch rate of the profile, as well as the Reynolds number, providing the following relation:

$$\begin{Bmatrix} \Delta c_n \\ \Delta c_m \end{Bmatrix} = \phi\big(\bar{w}_{3/4}, \bar{q}, \tau, M_\infty, Re\big) \tag{12}$$

Under the assumption that the Reynolds number plays a negligible role and that the analyses are conducted in incompressible conditions ($M_\infty = 0$), the model can be trained with $\bar{w}_{3/4}(\tau)$ and $\bar{q}(\tau)$ as unique inputs.

This framework exploits the Long-Short-Term Memory (LSTM) network to provide the relation in Eq. 12. The LSTM network is a prominent deep learning method designed for time sequence data, showing significant potential for addressing unsteady time-delayed effects in

system identification problems (see Ref. [17]). As a specialized variant of Recurrent Neural Networks (RNNs), the LSTM network overcomes the stability issues commonly faced by traditional RNNs, such as the vanishing gradient problem (see Ref. [18]). Unlike conventional unsteady aerodynamic modeling based on RNNs, where delay orders must be specified by the user, the LSTM network inherently considers time-delayed effects, simplifying the model training process considerably. Its architecture includes memory cells, input, output, and forget gates, which regulate the flow of information, enabling the network to maintain and update relevant information over extended time periods. This makes the proposed approach a promising tool for unsteady aerodynamic modeling. As evidence, Ref. [19] demonstrates that an LSTM network can effectively serve as a tool for defining a ROM capable of predicting aerodynamic loads and aeroelastic responses across various flight Mach numbers. In this paper, the LSTM network is trained using a regression model implemented with MATLAB® *Deep Learning Toolbox*™ functions (see Ref. [20]). The same toolbox allows the definition of the *Stateful Predict* block in Simulink® (highlighted in Fig. 6) that enables the integration of the neural network into the simulation framework shown in Fig. 5. Through this block, the LSTM network is able to dynamically generate output estimates as the input varies over time. Figure 10 provides the architecture of the trained LSTM neural network for sequence-to-sequence regression. It comprises two input features and two output features and includes two hidden LSTM layers, each containing 350 neurons. The training process utilized the Adam optimization algorithm (see Ref. [21]), a variant of stochastic gradient descent known for its adaptive learning rate properties, which effectively updates the network weights and biases based on the mean squared error (MSE) loss function calculated on the training data. To prevent overfitting, a validation check was incorporated into the training process. As detailed in Sec. 3, a portion of the collected data is reserved for validation purposes. The validation loss, calculated using the same MSE metric, is monitored alongside the training loss. Training is stopped if the validation loss increases relative to the training loss, indicating potential overfitting. This approach ensures the model maintained generalizability and robust performance on unseen data.

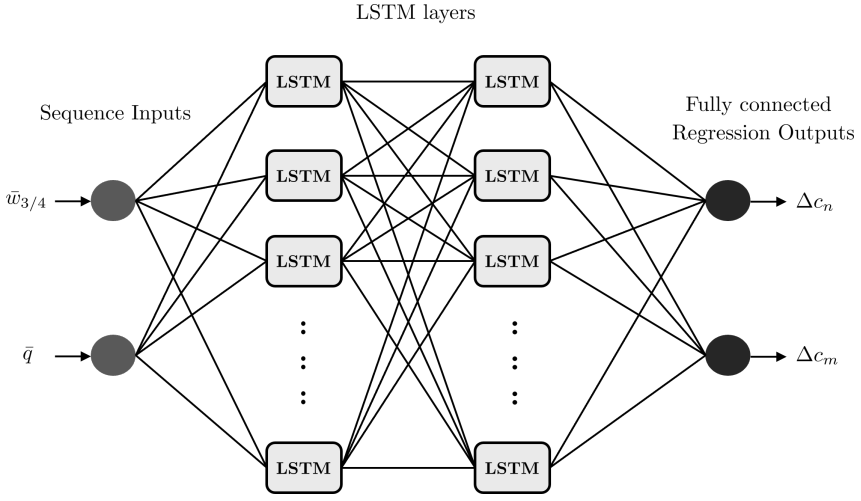

Figure 10: Architecture of the trained LSTM neural network.

In the present case, network training stopped after about 800 epochs, requiring approximately 40 minutes to complete. This duration was achieved utilizing the computational power of an average graphics card, specifically a mid-range GPU from the NVIDIA® GTX series. The efficiency of the process underscores the feasibility of conducting complex computations within

a reasonable timeframe, even without access to high-end, specialized hardware.

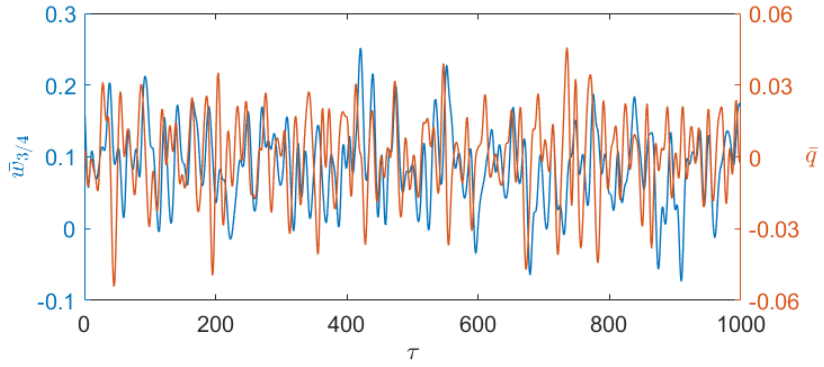

Figure 11: Inputs of the validation data set generated with $\alpha_0 = 5\,deg$, $A_h = 2.0 \cdot 10^{-2}$ and $A_\alpha = 1.0 \cdot 10^{-3}$.

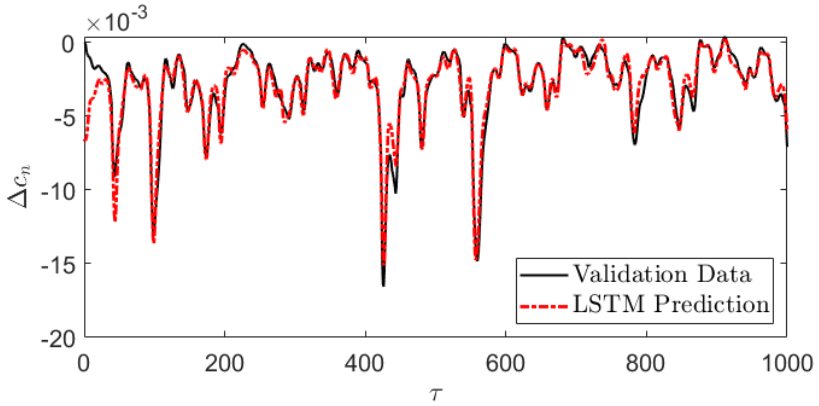

(a) Lift coefficient correction Δc_n

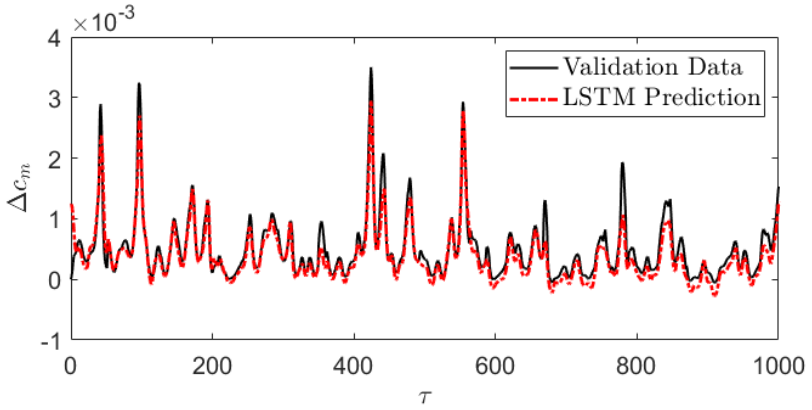

(b) Moment coefficient correction Δc_m

Figure 12: Comparison between the lift and moment coefficients predicted by the identified LSTM neural network and the validation output data corresponding to the inputs generated with $\alpha_0 = 5\,deg$, $A_h = 2.0 \cdot 10^{-2}$ and $A_\alpha = 1.0 \cdot 10^{-3}$ (see Fig. 11).

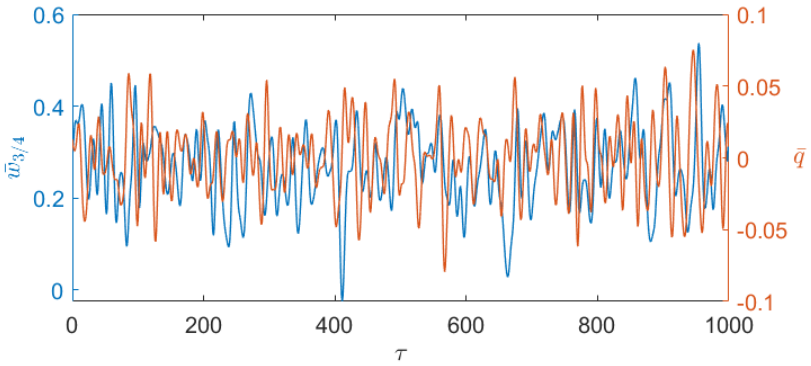

Figure 13: Inputs of the validation data set generated with $\alpha_0 = 15\,deg$, $A_h = 4.5 \cdot 10^{-2}$ and $A_\alpha = 2.3 \cdot 10^{-3}$.

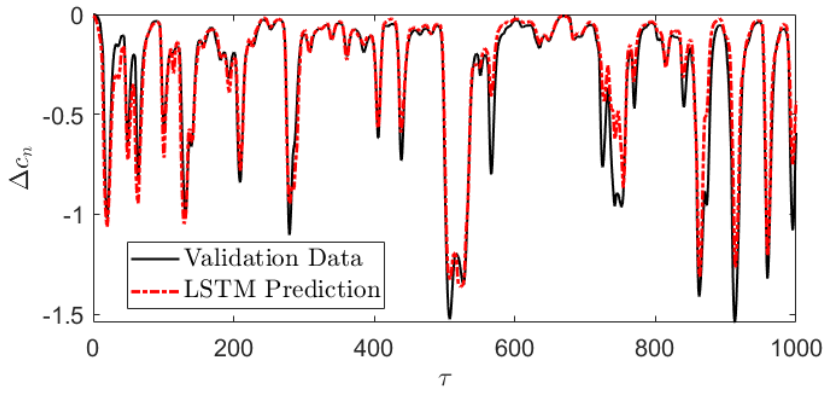

(a) Lift coefficient correction Δc_n

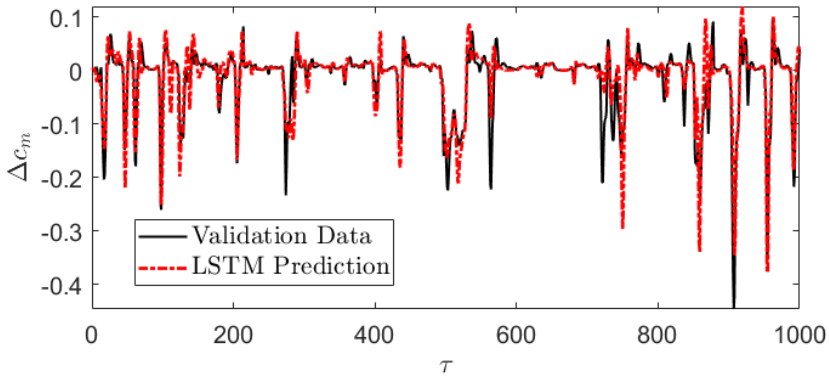

(b) Moment coefficient correction Δc_m

Figure 14: Comparison between the lift and moment coefficients predicted by the identified LSTM neural network and the validation output data corresponding to the inputs generated with $\alpha_0 = 15\,deg$, $A_h = 4.5 \cdot 10^{-2}$ and $A_\alpha = 2.3 \cdot 10^{-3}$ (see Fig. 13).

Since the validation dataset is not used to update the neural network parameters during training, it allows for an unbiased evaluation of the model predictive capabilities. Therefore, comparisons are presented below to assess the performance of the identified network using the validation data. Feeding the LSTM network with the input signals from the validation dataset shown in Fig. 11 (generated with $\alpha_0 = 5\,deg$, $A_h = 2.0 \cdot 10^{-2}$ and $A_\alpha = 1.0 \cdot 10^{-3}$) results in the responses shown in red in Fig. 12. The lift and moment coefficient corrections estimated by the network are compared with the validation outputs (black solid lines). In this case, the network is

able to estimate the nonlinear corrections with good efficiency, given the good overlap between the curves except for the first time instants. The model performance is generally good, with predictions in close agreement with reference results for most validation data. As the amplitudes considered increase, however, there is a slight deterioration in predictive accuracy. This can be seen in Fig. 14, which shows the responses estimated by the network based on the inputs shown in Fig. 11, generated with the values $\alpha_0 = 5\,deg$, $A_h = 2.0 \cdot 10^{-2}$ and $A_\alpha = 1.0 \cdot 10^{-3}$. Comparison with the dataset outputs reveals that the LSTM network tends to underestimate the coefficient corrections, particularly the moment correction.

5 RESULTS

This section presents the results of the methodology comparing the gust response of a wing with strip theory using three different models: linear, Beddoes-Leishman, and neural network. In particular, the results are presented for a number of flight points at which the combination of trim angle of attack and maximum gust amplitude is triggers the onset of dynamic stall resulting in loads reduction. Subsequently, a sensitivity analysis is conducted to assess the structural loads at various combinations of angle of attack and gust, with the results being compared with those obtained with the linear model. The analyses are conducted using a discrete gust as:

$$w_g(t) = \frac{1}{2} w_{g_a} \left[1 - \cos\left(\frac{2\pi U_\infty t}{L_g} \right) \right] \tag{13}$$

in which the gust length is such to maximize the gust load for the range of velocity considered in this study, that is $L_g = 35 b_{root}$. Table 2 provides the reference analyses used to display the effect of the dynamic stall and the capability of the neural network based ROM to predict the load reduction. The three cases are featured by the same product $q_D\,\alpha_0$. Figures 15, 16 and 17 show the dynamic response of the wing for the three different flight conditions. Prior to initiating the simulations, the initial conditions are set to the previously evaluated linear trim solution. The steady stall curve of the airfoil in Fig. 8 indicates that nonlinear models should be initiated with a different angle of attack to ensure consistent overall lift. To simply address this issue, the plots only show the difference with respect to the steady state, *i.e.* the perturbation of the first modal coordinate with respect to its steady state value either linear or nonlinear $\Delta q_1 = q_1 - q_{1_s}$, the second modal coordinate $\Delta q_2 = q_2 - q_{2_s}$, the vertical tip displacement $\Delta u_z(\mathbf{x}_{tip})$ and the wing root bending moment $\Delta M_x(\mathbf{x}_{root})$.

The results demonstrate that at low values of the angle of attack at the trim (case 1 in Fig. 15), the outcomes align with the linear attached flow model, regardless of the gust velocity value. This outcome is reflected in all three models (linear, Beddoes-Leishman, and LSTM network) for both modal response and derived quantities such as displacement at the tip and bending moment.

An increase in the value of the angle of attack at equilibrium, as seen in case 2 (Figs. 16), reveals that the dynamic response differs slightly from that of the linear case. The value of the modal coordinate q_1 reaches a lower peak in the simulation with the Beddoes-Leishman model. The LSTM-based model, despite its inability to perfectly describe the load reduction, does provide a reduction of the peak value of the first modal coordinate (see Fig. 16(a)). This is also reflected in the displacement at the tip and the trend of the wing root bending moment (see Fig. 16(c) and Fig. 16(d), respectively).

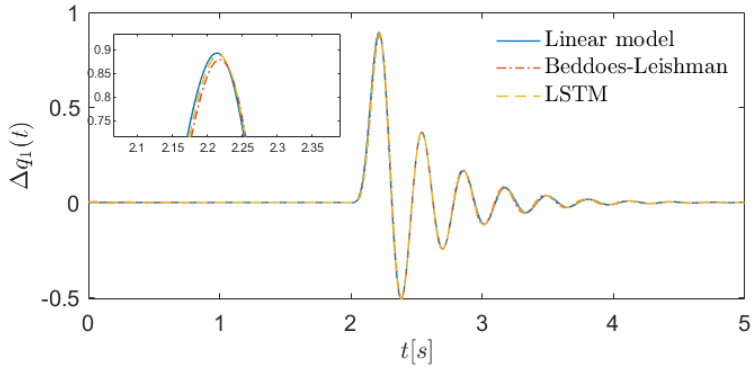

(a) $q_1(t)$

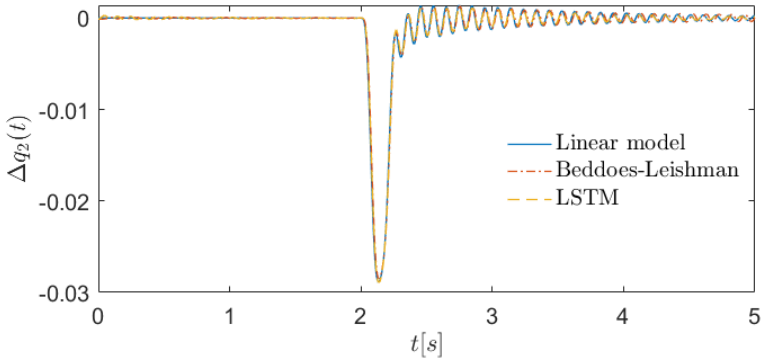

(b) $q_2(t)$

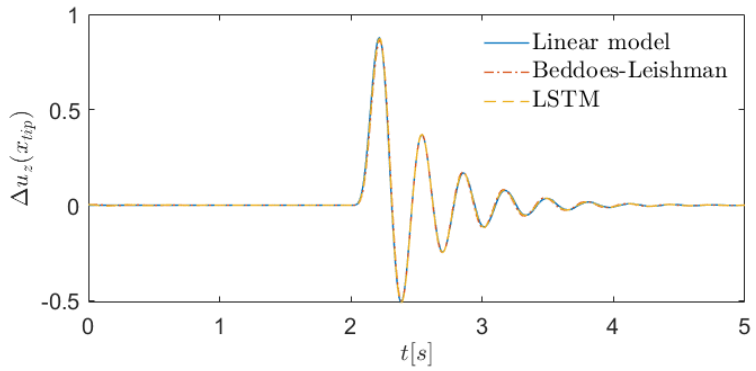

(c) tip displacement

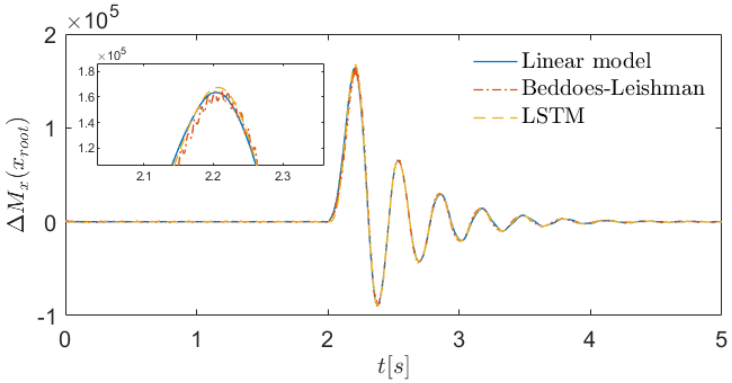

(d) $WRBM(t)$

Figure 15: Case 1: wing response.

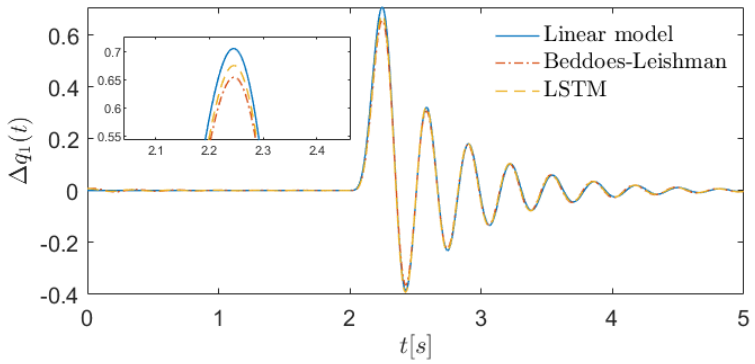

(a) $q_1(t)$

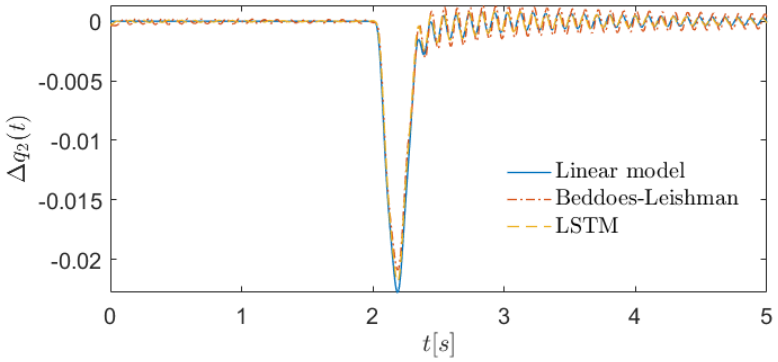

(b) $q_2(t)$

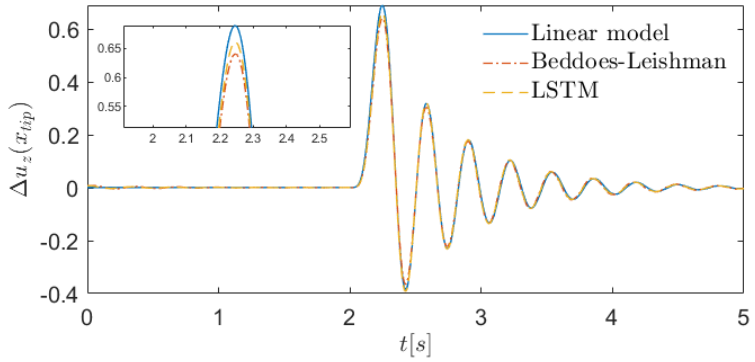

(c) tip displacement

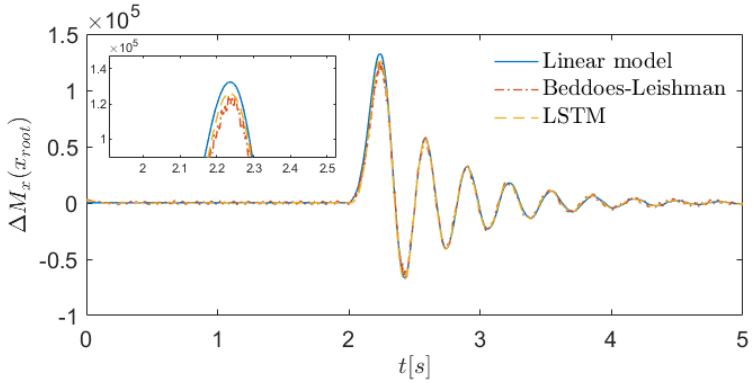

(d) $WRBM(t)$

Figure 16: Case 2: wing response.

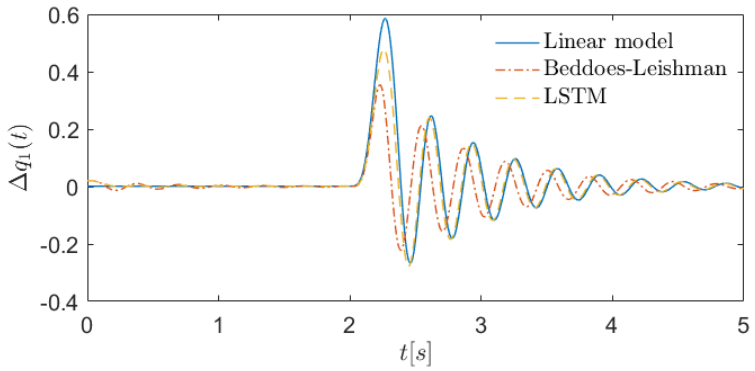

(a) $q_1(t)$

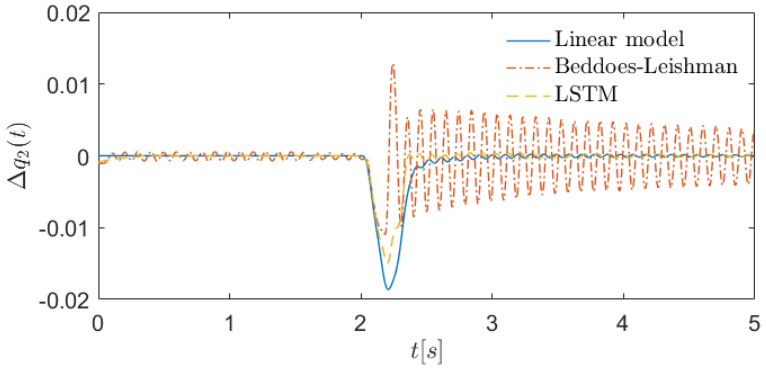

(b) $q_2(t)$

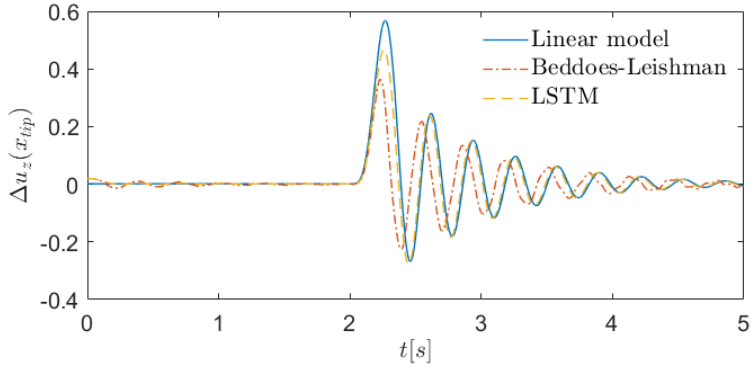

(c) tip displacement

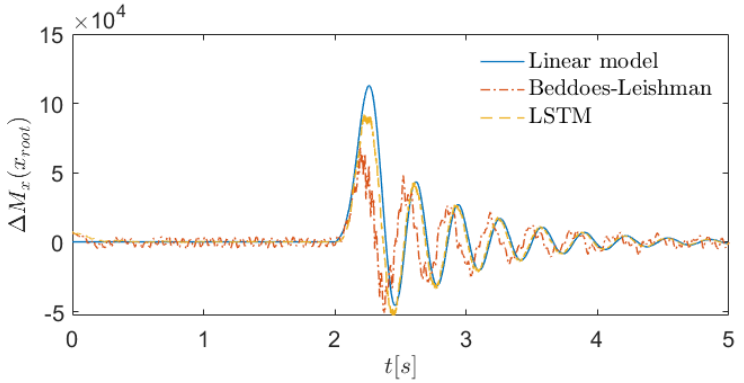

(d) $WRBM(t)$

Figure 17: Case 3: wing response.

case	$\alpha_0\,[deg]$	$U_\infty\,[m/s]$	$\rho\,[kg/m^3]$	$w_{g_a}\,[m/s]$
1	6.0	164.3	1.225	17.0
2	10.0	127.3	1.225	17.0
3	14.0	107.6	1.225	17.0

Table 2: Considered flight conditions.

Further increasing the angle of attack results in a discernible effect due to dynamic stall, as illustrated in case 3 in Figs. 17. As depicted in Fig. 17(a), this gives rise to a markedly lower first modal coordinate response. This effect is partially captured by the model with LSTM, which nevertheless returns a response of the first modal coordinate that lies somewhere between the linear case and the case with the Beddoes-Leishman model. This is reflected in the displacement trends at the tip and wing root bending moment. Furthermore, in the model using Beddoes-Leishman to describe the dynamic stall, there is synchrony between the dynamics of the flow separation point inherent in the Beddoes-Leishman modelling of the dynamic stall and the vibration modes with frequency lying between 3 ω_1 and 7 ω_1. This leads to a low amplitude and high frequency limit cycle oscillation as can be seen in Fig. 17(b). However, this type of behavior is not visible from the neural network model since the nonlinear aerodynamic model was identified for lower frequency bandwidth.

A response surface was then generated using the neural network model (Fig. 18) to examine the impact of dynamic stall in reducing the maximum wing root bending moment as a function of trim angle of attack within the range of 6 to 14 degrees and gust amplitudes between 11 and 19 m/s. Note that, in accordance with the approach presented, a variation in the angle of attack corresponds to a variation in dynamic pressure in order to ensure the same lift. In particular, the figure represents the perturbation due to the gust of the wing root bending moment obtained through the LSTM model, normalized with respect to the linear case. It can be observed that as both the initial angle of attack and the gust angle increase, the ratio in question decreases. However, it is evident that the sensitivity with respect to the trim attack angle is greater.

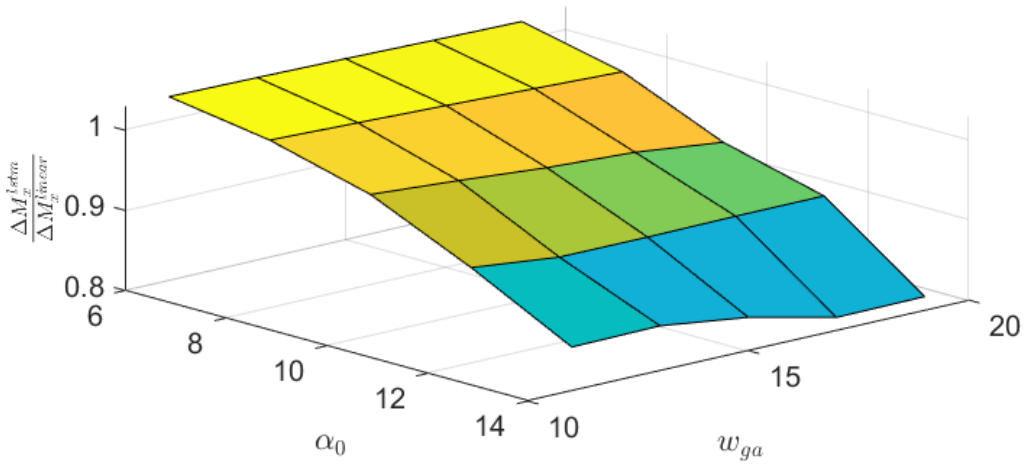

Figure 18: Response surface of load reduction given by dynamic stall.

6 CONCLUDING REMARKS

This study demonstrates the effectiveness of using a neural network-based reduced order model (ROM) to analyze the nonlinear gust response of a regional aircraft wing at high angles of attack

and under strong gust conditions. By combining strip theory with the Beddoes-Leishman unsteady aerodynamic model for initial training, the approach avoids the extensive computational effort required by traditional CFD simulations. The neural network-based ROM significantly reduces computational time while accurately predicting the aerodynamic loads and responses of the wing, making it practical for use in aircraft design. The model was successfully implementated in the Simulink environment, using Nastran structural data and strip theory. Training a single airfoil model simplifies the process and makes the method adaptable to different wing configurations, which is advantageous for applying the model to various aircraft designs without extensive retraining.

The results indicated that the use of a linear model may result in an overestimation of the root loads by 20%, which could lead to an overly conservative design phase. Furthermore, the methodology, although still in its incipient state, offers potential for improvement in several areas. One such area concerns the use of an aerodynamic dataset derived from computational fluid dynamics (CFD) simulations. Secondly, the methodology can be extended to consider the possibility of large displacements of the wing. Additionally, a linear aerodynamic model can be employed that is more closely aligned with industrial applications, such as the doublet lattice method, to replace the attached flow part obtained by strip theory.

7 REFERENCES

[1] Melis, D. J., Silva, J. M., Silvestre, M. A., et al. (2019). The effects of changing passenger weight on aircraft flight performance. *Journal of Transport & Health*, 13, 41–62.

[2] Albano, E. and Rodden, W. (1969). A doublet-lattice method for calculating lift distributions on oscillating surfaces in subsonic flows. *Journal of Aircraft*, 7(2), 279–285.

[3] Cary, A. W., Chawner, J., Duque, E. P., et al. (2021). Cfd vision 2030 road map: Progress and perspectives. In *AIAA Aviation 2021 Forum*. p. 2726.

[4] Wang, X., Van Kampen, E., Chu, Q. P., et al. (2019). Flexible aircraft gust load alleviation with incremental nonlinear dynamic inversion. *Journal of Guidance, Control, and Dynamics*, 42(7), 1519–1536.

[5] Schildkamp, R., Chang, J., Sodja, J., et al. (2023). Incremental nonlinear control for aeroelastic wing load alleviation and flutter suppression. *Actuators*, 12(7).

[6] Poussot-Vassal, C., Demourant, F., Lepage, A., et al. (2017). Gust load alleviation: Identification, control, and wind tunnel testing of a 2-d aeroelastic airfoil. *IEEE Transactions on Control Systems Technology*, 25(5), 1736–1749.

[7] Mannarino, A. and Mantegazza, P. (2014). Nonlinear aeroelastic reduced order modeling by recurrent neural networks. *Journal of Fluids and Structures*, 48, 103–121. ISSN 0889-9746.

[8] Li, K., Kou, J., and Zhang, W. (2019). Deep neural network for unsteady aerodynamic and aeroelastic modeling across multiple mach numbers. *Nonlinear Dynamics*, 96, 2157 – 2177.

[9] Saltari, F., Pizzoli, M., Gambioli, F., et al. (2022). Sloshing reduced-order model based on neural networks for aeroelastic analyses. *Aerospace Science and Technology*, 107708. ISSN 1270-9638. doi:https://doi.org/10.1016/j.ast.2022.107708.

[10] Nerattini, A., Pizzoli, M., Martinez-Carrascal, J., et al. (2024). Loads-based optimal fuel-usage strategy by using a neural-network-based reduced-order model for vertical sloshing. *SSRN*. doi:10.2139/ssrn.4786612.

[11] Leishman, J. G. and Beddoes, T. S. (1989). A semi-empirical model for dynamic stall. *Journal of The American Helicopter Society*, 34, 3–17.

[12] dos Santos, L. and Marques, F. (2021). Improvements on the beddoes–leishman dynamic stall model for low speed applications. *Journal of Fluids and Structures*, 106, 103375. ISSN 0889-9746.

[13] Huang, B., Wang, P., Wang, L., et al. (2021). A combined method of cfd simulation and modified beddoes-leishman model to predict the dynamic stall characterizations of s809 airfoil. *Renewable Energy*, 179, 1636–1649. ISSN 0960-1481.

[14] Laura, P. O. (2021). "blcode2.0". `https://github.com/laurapla/BLcode2.0`.

[15] Mazelsky, B. (1951). Numerical determination of indicial lift of a two-dimensional sinking airfoil at subsonic mach numbers from oscillatory lift coefficients with calculations for mach number 0.7. Tech. rep.

[16] Mazelsky, B. and Drischler, J. A. (1952). Numerical determination of indicial lift and moment functions for a two-dimensional sinking and pitching airfoil at mach numbers 0.5 and 0.6. Tech. rep.

[17] Hochreiter, S. and Schmidhuber, J. (1997). Long short-term memory. *Neural computation*, 9, 1735–80.

[18] Nelles, O. (2021). *Nonlinear system identification, from classical approaches to neural networks, fuzzy models, and gaussian processes*. Springer, 2 ed.

[19] Li, K., Kou, J., and Zhang, W. (2019). Deep neural network for unsteady aerodynamic and aeroelastic modeling across multiple mach numbers. *Nonlinear Dynamics*, 96, 1–21.

[20] Hudson Beale, M., Hagan, T., Martin, and Demuth, B., Howard (2023). *Deep Learning Toolbox*. The MathWorks, Inc., Natick, Massachusetts, United State.

[21] Kingma, D. P. and Ba, J. (2015). Adam: A method for stochastic optimization. In *International Conference on Learning Representations*.

COPYRIGHT STATEMENT